



FLUCOME 2009

10th International Conference on Fluid Control, Measurements, and Visualization
August 17–21, 2009, Moscow, Russia

A STUDY ON INTERACTION OF UNDEREXPANDED JET WITH THIN PLATE

M. Endo¹, E. Inamura², Y. Sakakibara³, and J. Iwamoto⁴

ABSTRACT

A supersonic jet is utilized in industries to cool a heated material, to blow the dust away from the product and so on, and also used for propulsion of space vehicle in aviation field. The jet is usually underexpanded or overexpanded, having a cell structure. When the jet impinges on materials having various geometries, the jet can oscillate and a noise radiates from it. In this paper, the underexpanded jet issuing from a convergent nozzle impinges normally on thin plate with elastic deformation and rigid thick plate. Oscillation of the jet and vibration of the plate were experimentally analyzed at different nozzle-plate spacings. The flow fields formed between the nozzle and the plates with various thicknesses were visualized by the shadowgraphy and compared to each other. Only the jet impinging on the rigid plate is numerically analyzed, compared with that by experiment. As a result, the relation was found between the flow pattern of the impinging jet and the deformation and vibration of the elastic plate.

Keywords: Supersonic Jet, Elasticity, Plate Shock, Screech Tone, Visualization

INTRODUCTION

A supersonic jet is used for propulsion of space vehicle in aviation field, and also utilized in industries to cool a heated material, to blow the dust away from the product and so on (Barsom J. M., 1968; Fieret J., et al., 1987; Aratani S., and Ojima N., 1991). Such a flow field can oscillate and radiate the high frequency noise known as a screech tone (Powell, A., 1988; Tamura, S. and Iwamoto, J., 1994). Furthermore, the impingement of the jet often leads to the fatigue failure of the structural materials.

So far, experimental and numerical studies have been carried out in order to analyze the shock-cell structure of the high-speed free jet (Tam C. K. W., 1988; Tamura S. and Iwamoto J., 1994), and the impinging jet has also been studied (Carling J. C. and Hunt B. L., 1974; Tamura S. and Iwamoto J., 1994; Sakakibara, Y. and Iwamoto, J., 2002). The radial underexpanded jet, which forms above on the wall, has been analyzed (Endo M., et al., 2000; Sakakibara Y., et al., 2005; Endo M., et al., 2006). Many studies have been vigorously made under the assumption that the wall of impingement is rigid. Thus, the deformation and the vibration of the wall were hardly considered.

¹ Corresponding author: Monozukuri Department, Tokyo Metropolitan College of Industrial Technology, email: endo@tokyo-tmct.ac.jp

² Monozukuri Department, Tokyo Metropolitan College of Industrial Technology

³ Department of Information and Arts, Tokyo Denki University

⁴ Department of Mechanical Engineering, Tokyo Denki University

In this paper, the underexpanded jet impinges normally on a thin plate with elastic deformation and furthermore on a thick plate which is not deformed. Oscillation of the jet and vibration of the plate were analyzed at different nozzle-plate spacings. The behaviour of the impinging jet on plates with various thicknesses was compared to each other.

EXPERIMENTAL CONSIDERATION

Figure 1 shows the experimental apparatus used in this study. The air compressed by the compressor goes through the demister and the air dryer, and then the cleaned air is supplied to the high pressure chamber installed in the soundproof room. The air in the high pressure chamber is stagnant because of its volume of 0.012m^3 and the diameter of 200mm, the pressure here being regulated by the valves. The converging nozzle, the diameter of which $D=10\text{mm}$, is screwed to the bottom of the chamber, its radius of curvature being $R=20\text{mm}$. The air in the chamber is accelerated along the converging nozzle and its velocity reaches that of sound at the nozzle exit, and then the high-speed jet issues into the surrounding air. The jet is underexpanded, and so the expansion and the compression of the jet repeat themselves as it flows downstream. In the present study, the underexpanded jet impinges normally on the thin plates of different thicknesses and the flow field formed between the nozzle and the plate is visualized using the shadowgraphy. The plates are made by aluminum, its thicknesses being $h=0.8, 1.0$ and 1.5mm . As shown in Fig. 2, the plate is $D_p=100\text{mm}$ in diameter and its rim is supported by the ring having step-shaped cross section, whose diameter $D_e=98\text{mm}$. The strain of the plate is measured with respect to the time using the semi-conductor type strain gauge glued on the surface of the reverse side "B". The thickest plate with $h=20\text{mm}$ is also employed. In this case the deformation of the plate caused by the jet impingement is considered to be negligible. The structure of the experimental setup is covered with sound-absorbent materials in order to reduce the reflection of the disturbance from the impinging jet.

The underexpanded jet is visualized by the shadowgraphy adopting the light ray emitted from the spark source, whose duration is 180ns. The camera focuses on the position of 60mm away from the jet axis. The flow visualization is carried out under the condition that the pressure in the high pressure chamber p_h is kept at three atmospheres $3.0p_a$ and that the nozzle to plate spacing L_s is varied from 13mm to 40mm at intervals of 1mm. Mach number of jet $M_j=1.358$ if the jet is fully expanded at the nozzle pressure ratio $p_h/p_a=3.0$, with the ratio of specific heats $\kappa=1.4$.

NUMERICAL SCHEME

The underexpanded jet impinging on the plate without an elastic deformation of the plate is numerically simulated. The computational flow field is assumed to be axisymmetric and Euler equation is employed as the governing equation and the flow field is solved using 2nd-order TVD scheme proposed by Yee (Yee H. C., 1987), with minmod function as a stable limiter function. The TVD scheme is usually employed in order to analyze the compressible flow phenomena. The authors also have used it as to simulate numerically the underexpanded impinging jet on a flat plate and the good agreement was found between the experiment and the calculation concerning about the oscillation of the impinging jet (Sakakibara, Y. and Iwamoto, J., 2002). In the present study, the same scheme is adopted with boundary conditions adjusted to the specific problem.

The computational region used in this study is covered with a structured mesh. The radial distance of the region is 7.5 diameters of the converging nozzle, where 150 computational grids are clustered towards the jet axis. Along the jet axis there are 100 grids at uniform intervals. The critical condition estimated from the stagnant properties in the high pressure chamber is specified at the exit plane of the nozzle. The boundary condition is given to be reflective at the jet axis. At the other boundaries the Riemann variables are kept constant. As the initial conditions, the atmospheric condition with zero velocity is given on the computational flow field, and the critical condition at the nozzle exit in the region surrounded by the jet

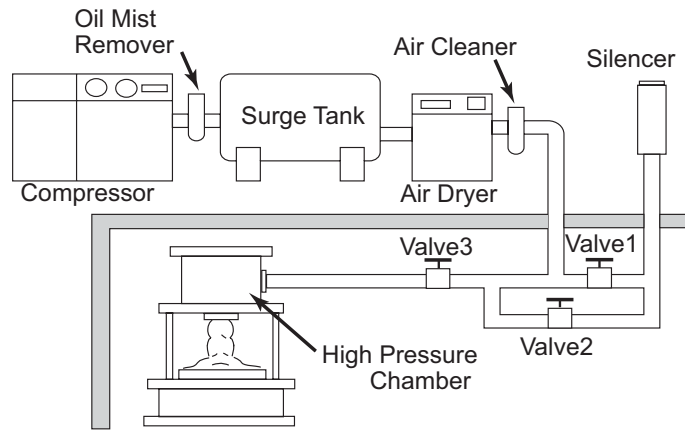


Fig. 1. Schematic of Experimental Apparatus

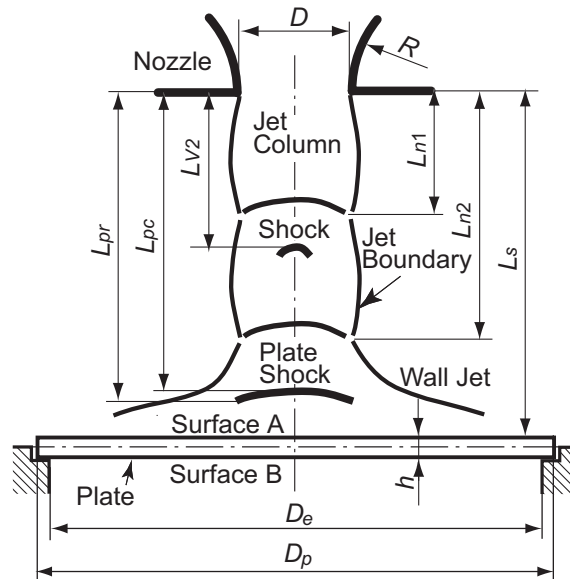


Fig. 2. Thin Plate

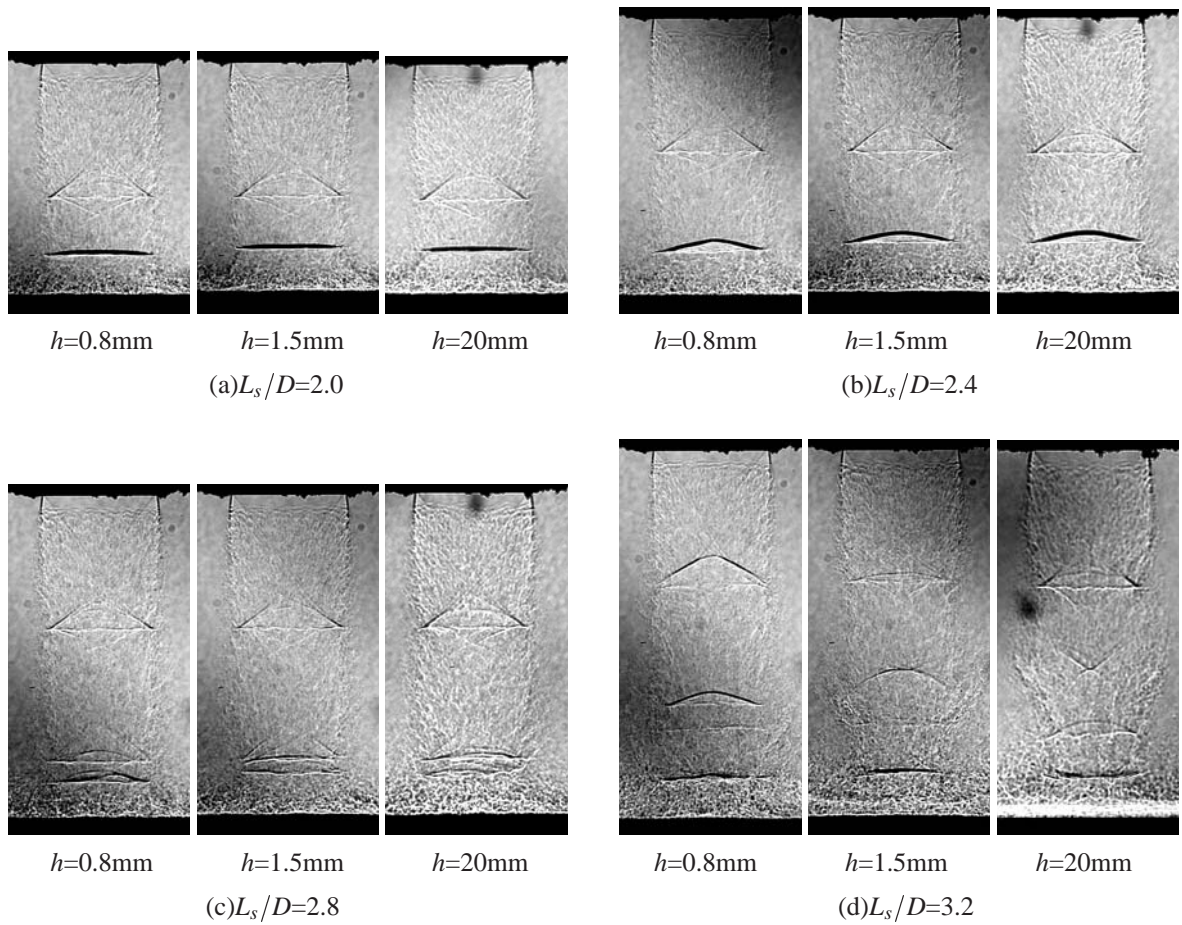


Fig. 3. Shadowgraph Pictures of Impinging Jet on Plate with Different Thicknesses

axis, the nozzle exit, the plate and the line through the nozzle lip running parallel to the jet axis.

RESULTS AND DISCUSSION

Visualization of Flow Field

Figure 3 shows the shadowgraph pictures of the underexpanded jet impinging on the plate with different thicknesses. The shadowgraph pictures shown on the left, middle and right in each figure indicate the flow pattern for $h=0.8\text{mm}$, 1.5mm and 20mm , respectively. The jet issues from the upper nozzle and impinges on the downstream plate. The jet boundary appears to become obscure as the jet goes downstream. At $L_s/D=2.0$, the flat-type plate shock is formed above the plate. The shape of the plate shock changes to the convex type as the nozzle-plate spacing increases. With further increase in the nozzle-plate spacing the plate shock jumps into the 3rd cell as shown in the pictures at $L_s/D=2.8$. At $L_s/D=3.2$, the flow pattern differs somewhat from those at the other L_s/D and another shock is observed to appear in the 2nd cell, which has various shapes. Three shadowgraph pictures are taken at random under the same condition and the location of the shock waves is measured as shown in Fig. 2.

The result for $h=0.8\text{mm}$ is shown in Fig. 4. The abscissa is the nozzle-plate spacing and the ordinate the location of the shocks measured from the nozzle exit plane. These distances are nondimensionalized by the diameter of the nozzle D . The empty plots denote the locations of the rim of the shock and the

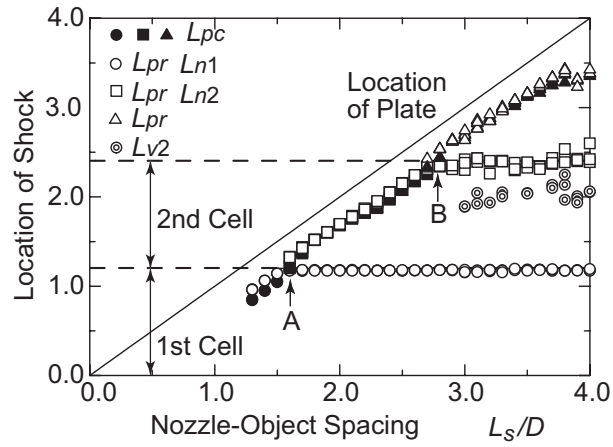


Fig. 4. Locations of Shocks at $h=0.8\text{mm}$

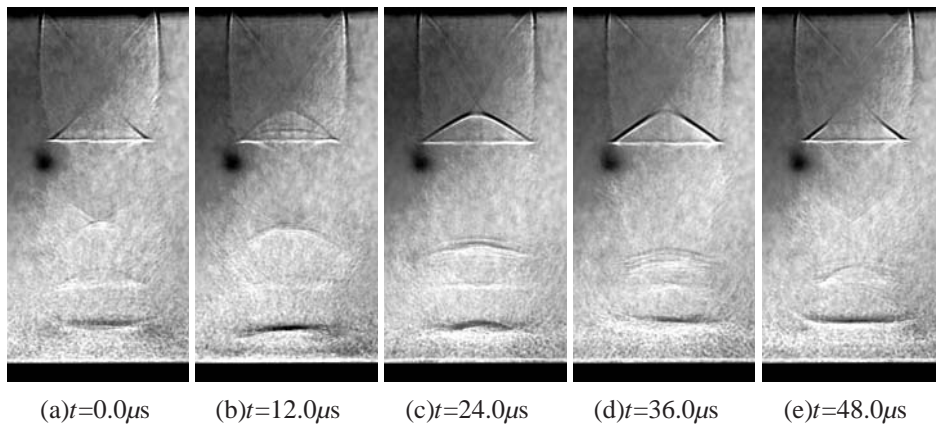


Fig. 5. Shadowgraph Pictures of Impinging Jet on Plate with Thickness of $h=0.8\text{mm}$ at $L_s/D=3.2$

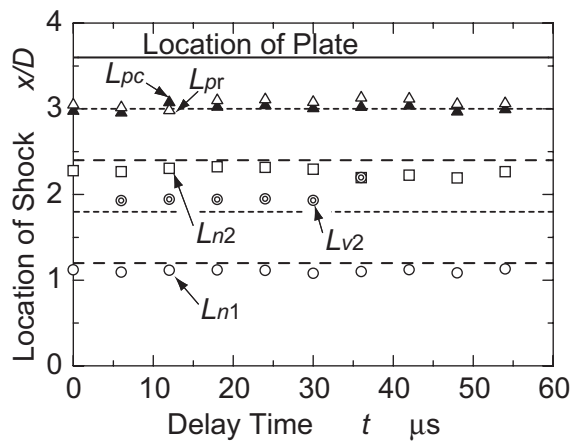
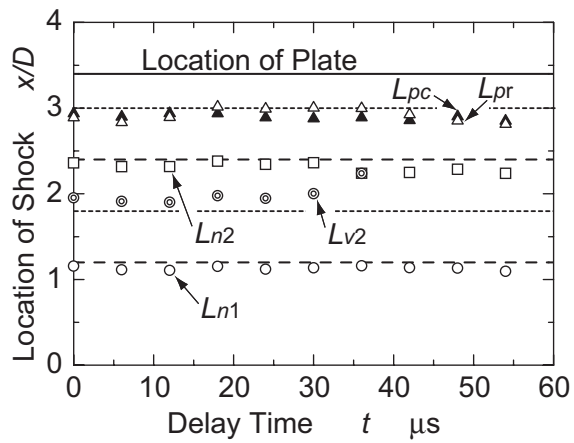
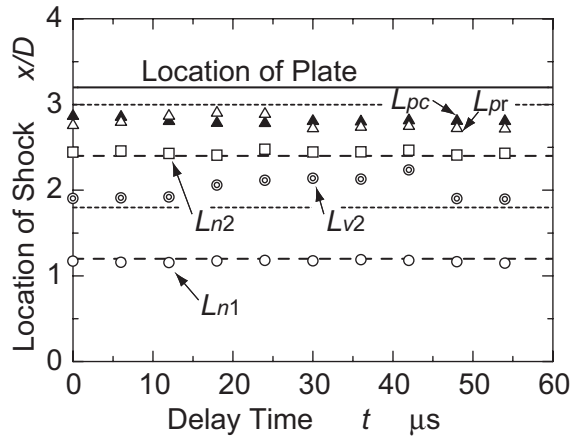


Fig. 6. Geometry and Location of Shock

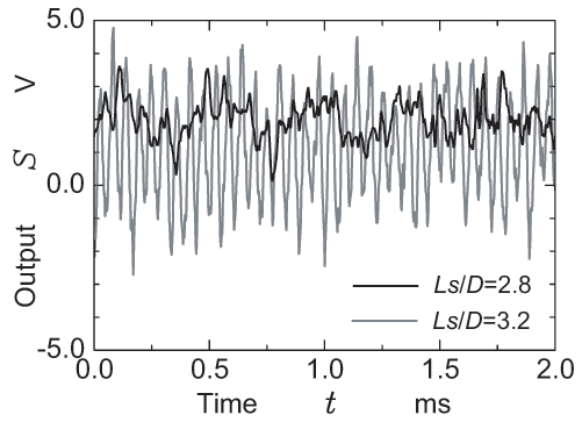
solid ones the center. The double circle means the locations of the shock in the 2nd cell L_2 as shown in Fig. 3(d). The solid line is the location of the plate L_s . The dashed lines running parallel to the abscissa is the location of the node of cell estimated by Tam's theory (Tam C. K. W., 1988). Using Tam's theory, $L/D=1.20$ for $M_j=1.358$, where L is the length of cell. As shown in Fig. 4, the plate shock is flat in the expansion region of the jet and convex in the compression region. The location of the plate shock suddenly changes near the node of cell at the nozzle plate spacings labeled by "A" and "B". The 1st node is stable at stationary location, while the 2nd node changes with time as the plotted values are scattered. And also, the shock formed in the 2nd cell is considered to fluctuate. In particular, the 1st node oscillates slightly at $L_s/D > 3.0$, where the shock appears in the 2nd cell. Such a flow pattern is observed regardless of the plate thickness. The sudden change of the location of the plate shock near the node occurs at the shorter nozzle-plate spacing as the jet impinges on the thinner plate, which is due to a larger deflection of the plate caused by jet impingement, i.e. the nozzle-plate spacing becomes longer near the center of plate than the length in case of the rigid plate. As can be seen in Fig. 3(c), the 2nd cell is completely formed and the plate shock is located below the node of 2nd cell regardless of the thickness of the plate. The spacing between the node and the plate shock at $h=0.8\text{mm}$ is larger than that at $h=1.5\text{mm}$ or 20mm , which means that the sudden change of the location of the plate shock occurs at the shorter nozzle plate spacing in case of the thinner plate.

Figure 5 shows the shadowgraph pictures of the impinging jet on the thin plate with $h=0.8\text{mm}$ at the nozzle-plate spacing of $L_s/D=3.2$. These are the pictures at the instant delayed by t measured from the application of the trigger signal of the strain gauge on the plate. The pictures are taken 30 times on the same film under the same condition, i.e. the ensemble-averaged pictures are obtained. In the downstream region of the 1st cell the oblique shock grows towards the jet boundary. The length of the 1st cell is maintained constant with time, while the strength of the oblique shock is fluctuated. The fluctuation is recognized by observing the thickness of the oblique shock in each picture. The shock formed in the 2nd cell at $t=0.0\mu\text{s}$ as shown in Fig. 5(a) moves downstream as its diameter becomes large and approaches the downstream node of the 2nd cell. The downstream node and the plate shock in the 3rd cell also change in shape, which synchronizes with the motion of the shock in the 2nd cell.

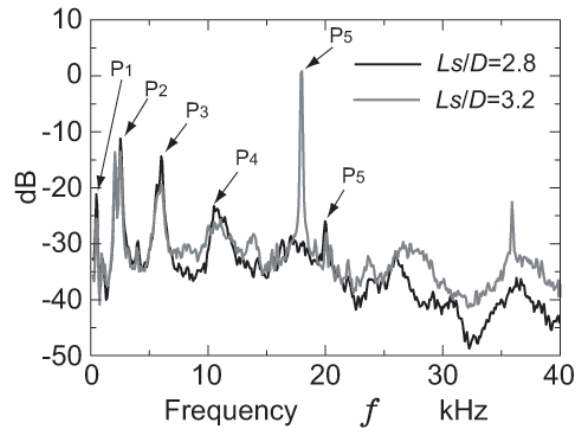
Analyzing such shadowgraph pictures as shown in Fig. 2, the locations of the node of cell and shocks are plotted against the time. Figure 6 shows the results at $L_s/D=3.2, 3.4$ and 3.6 , where the solid line means the location of the plate and the dashed ones the theoretical location of the node. A half value of a theoretical cell length is shown by the dotted lines in the 2nd and 3rd cells.

In Fig. 6(a), the location of the downstream node of the cell compares well to the result of Tam's theory and the length of the 1st cell is maintained constant, while that of the 2nd cell is slightly fluctuated. The shock formed in the 2nd cell slowly goes downstream and suddenly moves from $t=12\mu\text{s}$ to $18\mu\text{s}$. After that, the velocity becomes low again and the moving shock accelerates at about $t=45\mu\text{s}$ and then, it changes into the downstream node of the 2nd cell. At $t=48\mu\text{s}$, the new moving shock appears at $x/D \doteq 1.9$. As can be seen in Fig. 5(a), the plate shock, which is of slightly concave type at $t=0.0\mu\text{s}$, is changed into that of convex type at $t=12\mu\text{s}$. The velocity of the moving shock suddenly changes at the instant when this change in shape occurs. The convex-type plate shock returns to the slightly concave type at $t=30\mu\text{s}$. As mentioned above, the flow field is fluctuated with a period of about $60\mu\text{s}$.

In Fig. 6(b), the moving shock is formed at $x/D \doteq 1.9$ and goes downstream with stepped change in velocity, replacing the weak shock at the downstream node of the 2nd cell. After that, the new moving shock does not appear again. The amplitude of the oscillation of the downstream node of the 2nd cell is larger than that at $L_s/D=3.2$. The plate shock changes in shape in the same way as it does at $L_s/D=3.2$ and the duration of being the concave-shape becomes longer. In Fig. 6(c), the convex type shock is formed except at $t=12\mu\text{s}$. This is caused by the location of the plate shock, which moves from expansion region to compression one as the nozzle-plate spacing increases. The appearance of the moving shock lasts shorter in case of the larger nozzle-plate spacing.



(a) Output from Strain Gauge



(b) Frequency

Fig. 7. Vibration of Plate at $L_s/D=2.8$ and 3.2

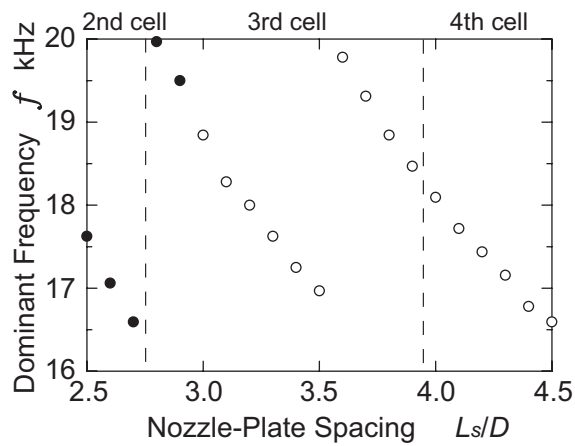


Fig. 8. Variation of Dominant Frequency

Vibration of Plate

The vibration of the plate is measured using the strain gauge glued at the center of the plate at different nozzle-plate spacings. The output signal is recorded through A/D converter in three seconds. Figure 7(a) shows the signal from the strain gauge for the nozzle-plate spacings $L_s/D=2.8$ and 3.2, and the FFT analysis of the signal is also shown in Fig. 7(b). As can be seen in Fig. 7(a), the plate is vibrated comparatively at random for $L_s/D=2.8$, its amplitude being nearly 4.0v. A few dominant frequency components are included as shown in Fig. 7(b), which are P_1 of 0.47kHz, P_2 of 2.5kHz, P_3 of 6.0kHz, P_4 of 11kHz and P_5 of 20kHz. For $L_s/D=3.2$, the plate is periodically vibrated and its amplitude reaches 8.0v which is about two times larger than that for $L_s/D=2.8$. P_5 of 18kHz dominates the vibration of the plate and the other components from P_1 to P_4 are less influential. Thus, The dominant frequency components except for P_5 are maintained constant regardless of the nozzle-plate spacing and the pattern of the vibration changes at $L_s/D=3.0$. This is caused by the change of the flow pattern that the flow field oscillates periodically at $L_s/D>3.0$. The components from P_1 to P_4 correspond to the results obtained through the theoretical analysis under the assumption that the plate is supported at its rim by the base.

The change of the component P_5 against the nozzle-plate spacing is shown in Fig. 8. The empty plot means the component P_5 dominates the vibration of the plate more than the other components. The range divided with the dashed lines running parallel to the ordinate shows the number of cells which comprise the impinging jet; e.g. the 2nd cell is completely formed and the 3rd cell is partly in the nozzle plate spacing ranging from $L_s/D=2.8$ to 3.9. The frequency of P_5 gradually reduces as the nozzle-plate spacing increases and reaches about 16.5kHz at $L_s/D=2.7$. At $L_s/D=2.8$ the frequency jumps to 20.0kHz. After that, the frequency decreases to about 17kHz and the frequency jump occurs again, and then reaches 19.8kHz at $L_s/D=3.6$. Such a sawtooth-type change of the dominant frequency was observed in the measurement of the noise emitted from the impinging jet by S. Tamura and J. Iwamoto (Tamura, S. and Iwamoto, J., 1994).

As can be seen in Fig. 4, the plate shock located in the 2nd cell at $L_s/D<2.7$ jumps into the 3rd cell at $L_s/D=2.8$. Thus, the location of the plate shock affects the frequency of the component P_5 . However the frequency jump does not occur at $L_s/D=3.9$, which is considered to be caused by the deformation of the 4th cell. At $L_s/D=3.5$ the plate shock is located at the middle point of the 3rd cell as can be seen in Fig. 3. As shown in Fig. 6(b) for $L_s/D=3.4$, the duration of the convex-type plate shock is equal to that of the concave type. And so, the plate shock is located at the border between the expansion and compression regions of the cell. Since the pressure distribution on the plate is greatly affected by the location of the plate shock, the frequency of P_5 is considered to change suddenly.

The same analyses is performed for other thin plates with $h=1.0$ and 1.5mm. The comparatively random vibration occurs for $L_s/D<3.0$ and the higher frequency components, which correspond to the component P_1 to P_4 respectively, appear than that of $h=0.8$ mm; e.g. the lowest component P_1 is 0.56kHz at $h=1.0$ mm and 0.93kHz at 1.5mm. The output from the strain gauge reduces as the stiffness of the plate increases due to the thick of the plate. Regardless of the plate thickness, the frequency of P_5 is changed from 16kHz to 20kHz as shown in Fig. 8 for $L_s/D>3.0$. Thus, the component P_5 is considered to be induced by the oscillation of the impinging jet. Two frequency jumps occur as shown in Fig. 8 at longer nozzle-plate spacing than that of $h=0.8$ mm. This is due to the stiffness of the plate. The deflection at the center of plate are about 0.7mm at $h=0.8$ mm, 0.3mm at $h=0.8$ mm and 0.1mm at $h=1.5$ mm, respectively. Because the average curvature radius of the plate at $h=0.8$ mm is about 3.4m, the flow pattern at certain L_s/D with this plate can be considered to be similar to that at larger L_s/D with the other plates.

Numerical Simulation of Flow Field

The numerical simulation is carried out of the impinging jet on the rigid plate. Figure 9 shows the pressure history at the center of the plate p_c at $L_s/D=3.2$. The abscissa is the time elapsing from arbitrary instant. The pressure in the ordinate is nondimensionalized by the ambient pressure. The pressure

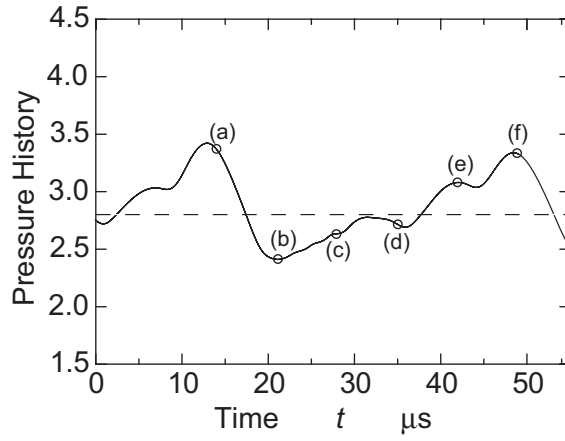


Fig. 9. Pressure History at Center of Plate

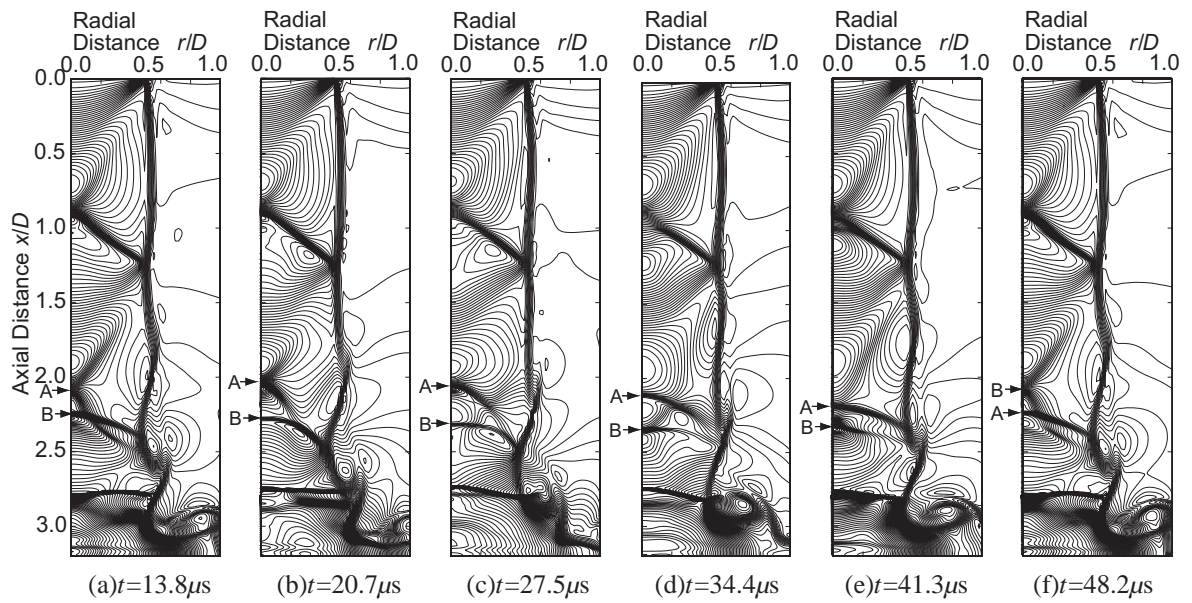


Fig. 10. Density Contours of Flow Field of Jet Impinging on Rigid Plate at $L_s/D=3.2$

periodically changes around the pressure at the high pressure chamber of $p_h/p_a=3.0$. The period of the flow oscillation is $36\mu s$ as can be seen in Fig. 9, it being shorter than that by the experiment. The average pressure is $\bar{p}_c/p_a\div 2.8$ which is shown by the dashed line. The pressure is maximum at $t\div 13\mu s$, which is larger than that in the high pressure chamber. It is suddenly dropped and reaches the minimum pressure $p_c/p_a\div 2.4$ at $t\div 21\mu s$. After that, the pressure gradually rises through stairs-like change, and then arrives at the maximum pressure $p_c/p_a\div 3.4$ again. Thus, the pressure at the center of plate periodically changes with amplitude of 1.0.

Figure 10 shows the density contours of the impinging jet. The nozzle is located at the top and the plate at the bottom of the figure, the ordinate being the jet axis. Each figure shows the flow pattern at the empty plot in Fig. 9. As can be seen in these figures, the shock formed in the 2nd cell gradually moves downstream and then replaces the weak shock at the node of cell. Thus, the numerical results simulate well the flow pattern of the impinging jet shown in Fig. 5. The expansion wave from the upstream node of the 2nd cell is reflected at the jet boundary and the compression wave is concentrated, and then the oblique shock is formed in the cell. The jet boundary is deformed downstream by the vortex generated in the vicinity of the nozzle lip. The barrel-like shape of the 2nd cell is changed and the jet boundary becomes partly concave and partly convex. The locally deformed boundary moves downstream.

The shock "A" starts to form at the center of the cell at $t\div 13\mu s$ as shown in Fig. 10(a), when p_c is maximum. It goes downstream with the local deformation and grows towards the jet boundary. The shock "B" formed at the downstream node of the 2nd cell is located downstream of the shock "A", its shape being convex. In Fig. 10(b), when the pressure is minimum, the center of the shock "B" flattens and becomes stronger. The shock "B" weakens as the shock "A" grows toward the jet boundary and the center pressure of the plate gradually increases. The distance between shocks "A" and "B" becomes short and the shock "B" changes into relatively strong compression wave as shown in Fig. 10(e). The compression wave quickly moves upstream as the locally deformed jet boundary goes downstream, and then the shock "B" starts to form at $x/D\div 2.0$ on the jet axis as shown in Fig. 10(f). Thus, there are two shocks "A" and "B" in the 2nd cell and the formation, the movement and the reduction of the strength of the shocks repeat themselves alternatively. The behaviour of the two shocks is caused by deformation of the jet boundary due to the convection of vortex.

CONCLUSIONS

The underexpanded jet impinges normally on the plates with different thicknesses and the flow field is experimentally and numerically analyzed. The strain and the deflection at the center of the plate are measured and the vibration of the plate is analyzed. The relation of the flow pattern with the vibration of the plate is discussed. As a result, the following conclusions are drawn;

- (1) The thickness of the impinging plate does not affect flow pattern but the nozzle-plate spacing where the flow pattern changes because of the deflection of the plate.
- (2) The flow pattern is transformed depending on the number of cell comprising the cell structure of impinging jet. The change occurs at the nozzle-plate spacing $L_s/D\div 3.0$ in the experiment.
- (3) The experimental analysis shows the plate vibration for $L_s/D < 3.0$ is dominated by the natural frequencies of the plate, while the component of 18kHz for $L_s/D > 3.0$. This component changes in sawtooth type ranging from 16kHz to 20kHz.
- (4) The calculation simulates the to-and-fro behaviour of two shocks in the 2nd cell and the periodical motion synchronizes with the change of the pressure on the plate.

ACKNOWLEDGMENTS

The experiments described above were made in cooperation with Messrs. T. Aoki, D. Yasuda and N. Furuta. The authors would like to thank their assistances.

REFERENCES

- Aratani, S., and Ojima N. (1991), "Effect of shock waves on fracture and quenching in tempered glass", Proceedings of 8th International Symposium of Shock Waves, 1277-1282.
- Barsom, J., M. (1968), "Fracture of Tempered Glass", Journal of American Ceramics Society, **51**, 75-78.
- Carling, J. C. and Hunt, B. L. (1974), "The Near Wall Jet of a Normally Impinging, Uniform, Axisymmetric, Supersonic Jet", Journal of Fluid Mechanics, **66**(1), 159-176.
- Endo, M., et al. (2000), "A Study of Radial Underexpanded Jets", Proceedings of 9th International Symposium on Flow Visualization, Paper No. 406.
- Endo, M., et al. (2006), "A Study of Time-Averaged Cellular Shape of Underexpanded Radial Jet", Transactions of the Japan Society of Mechanical Engineers, Series B, **72**(720), 35-40 (in Japanese).
- Fieret, J., et al. (1987), "Overview of Flow Dynamics in Gas-Assisted Laser Cutting", SPIE High Power Lasers, **801**, 243-250.
- Powell, A. (1988), "The sound-producing oscillations of round underexpanded jets impinging on normal plates", Journal of Acoustical Society of America, **83**(2), 515-533.
- Sakakibara, Y., et al. (2005), "A Study on Flow Field of Radial Underexpanded Jet", Transactions of the Japan Society of Mechanical Engineers, Series B, **71**(712), 94-99 (in Japanese).
- Sakakibara, Y. and Iwamoto, J. (2002), "Oscillation of Impinging Jet with Generation of Acoustic Waves", International Journal of Aeroacoustics, **1**(4), 385-402.
- Tam, C. K. W. (1988), "THE SHOCK-CELL STRUCTURES AND SCREECH TONE FREQUENCIES OF RECTANGULAR AND NON-AXISYMMETRIC SUPERSONIC JETS", AIAA, J. Sound and Vibration, **121**(1), 135-147.
- Tamura, S. and Iwamoto, J. (1994), "Study on the Noise Generated from Underexpanded Free and Impinging Jet", Transactions of the Japan Society of Mechanical Engineers, Series B, **60**(579), 283-289 (in Japanese).
- Yee, H. C. (1987), "Upwind and Symmetric Shock-Capturing Schemes", NASA TM 89464.